DR. MARIA NOEL URRUTIA (Orcid ID : 0000-0003-4274-9688)
DR. SERGIO BONESI (Orcid ID : 0000-0003-0722-339X)
MISS MARIANA VIGNONI (Orcid ID : 0000-0003-4506-7527)
DR. ALEXANDER GREER (Orcid ID : 0000-0003-4444-9099)
DR. ANDRÉS HÉCTOR THOMAS (Orcid ID : 0000-0002-8054-7799)

Article type : Special Issue Research Article

SPECIAL ISSUE RESEARCH ARTICLE

Mono- and *Bis*-Alkylated Lumazine Sensitizers: Synthetic, Molecular Orbital Theory, Nucleophilic Index, and Photochemical Studies†

María José Sosa,[1] María Noel Urrutia,[1] Patricia L. Schilardi,[1] Matías I. Quindt,[2] Sergio Bonesi,[2] Dobrushe Denburg,[3] Mariana Vignoni,[1] Alexander Greer,[4,5,*] Edyta M. Greer,[3,*] Andrés H. Thomas[1,*]

[1] *Instituto de Investigaciones Fisicoquímicas Teóricas y Aplicadas (INIFTA), Departamento de Química, Facultad de Ciencias Exactas, Universidad Nacional de La Plata (UNLP), CCT La Plata-CONICET, Diagonal 114 y 64, (1900) La Plata, Argentina.*

[2] *CIHIDECAR-CONICET, Departamento de Química Organica, FCEyN, Universidad de Buenos Aires, Pabellón 2, 3er Piso, Ciudad Universitaria, Buenos Aires, Argentina.*

[3] *Department of Natural Sciences, Baruch College, City University of New York, New York, NY*

[4] *Department of Chemistry, Brooklyn College, City University of New York, Brooklyn, New York 11210, United States.*

[5] *Ph.D. Program in Chemistry, The Graduate Center of the City University of New York, 365 Fifth Avenue, New York, New York 10016, United States.*

*** Corresponding authors email:** agreer@brooklyn.cuny.edu (Alexander Greer), edyta.greer@baruch.cuny.edu (Edyta M.Greer), athomas@inifta.unlp.edu.ar (Andrés H. Thomas)

†This article is part of a Special Issue commemorating the XIV ELAFOT Conference held from November 11th to 14th, 2019 in Viña del Mar, Chile.

ABSTRACT

Mono- and *bis*-decylated lumazines have been synthesized and characterized. Namely, mono-decyl chain [1-decylpteridine-2,4(1,3*H*)-dione] **6a** and *bis*-decyl chain [1,3-didecylpteridine-2,4(1,3*H*)-dione] **7a** conjugates were synthesized by nucleophilic substitution (S_N2) reactions of lumazine with 1-iododecane in *N,N*-dimethylformamide (DMF) solvent. Decyl chain coupling occurred at the N^1 site and then the N^3 site in a sequential manner, without DMF condensation.

Molecular orbital (MO) calculations show a *p*-orbital at N^1 but not N^3, which along with a nucleophilicity parameter (*N*) analysis predict alkylation at N^1 in lumazine. Only after the alkylation at N^1 in **6a**, does a *p*-orbital on N^3 emerge thereby reacting with a second equivalent of 1-iododecane to reach the dialkylated product **7a**. Data from NMR (^{1}H, ^{13}C, HSQC, HMBC), HPLC, TLC, UV-vis, fluorescence, and density functional theory (DFT) provide evidence for the existence of mono-decyl chain **6a** and *bis*-decyl chain **7a**. These results differ to pterin *O*-alkylations (kinetic control), where *N*-alkylation of lumazine is preferred and then to dialkylation (thermodynamic control), with an avoidance of DMF solvent condensation. These findings add to the list of alkylation strategies for increasing sensitizer lipophilicity for use in photodynamic therapy.

INTRODUCTION

Pteridines in their multiple forms are widespread in biological systems playing various roles (1,2,3,4). Within this family of heterocyclic compounds (5), pterins are those compounds derived from 2-aminopteridine-4(3*H*)-one (native pterin; denoted Ptr) and lumazines are those derived from pteridine-2,4(1,3*H*)-dione (native lumazine; denoted Lum) (Fig. 1). The parent Ptr and Lum are poorly soluble in aqueous and organic solvents. Nonetheless, they are present in living systems in different redox states and fall into three classes: fully oxidized (or aromatic) pterins, dihydro and tetrahydro derivatives. The latter derivatives are important biologically, but are photochemically inactive due to fast nonradiative deactivation of their singlet excited states (6). On the other hand oxidized pteridines are able to fluoresce, undergo photooxidation and produce reactive oxygen species (7). Moreover, these compounds are efficient photosensitizers and are able to photoinduce the oxidation of biomolecules (8,9) and cell death (10,11,12). Ptr, the parent and unsubstituted compound of oxidized pterins (Fig. 1), freely passes across phospholipid membranes of large unilamellar vesicles, but can photoinduce oxidation of lipids enriched in polyunsaturated fatty acids (PUFAs) (13).

<Figure 1>

Recently, we reported on the conjugation of a decyl chain to Ptr to increase its solubility in organic solvents and also facilitate the binding to phospholipid membranes (14,15). Three key findings were: (i) only one mole of 1-iododecane was added to Ptr, that is, only the mono-decyl-chain and not *bis*-decyl-chain pterins were obtained. (ii) Kinetic control was observed in the regioselective *O*-alkylation instead of *N*-alkylation of the Ptr. Higher percent yields were found for the 4-(decyloxy)pteridin-2-amine (*O*-decyl-Ptr **1**) (37%) than for the *N*-decylated

pterin **3** (20%) (Fig. 2), where no "walk" rearrangements were found because of high energy barriers. (iii) A shortcoming in the synthesis was that the poor solubility of Ptr required a solvent such as *N,N*-dimethylformamide (DMF) which then led to DMF condensation onto the amine group, thereby forming *O*-decylated pterin **2** and *N*-decylated pterin **4** (Fig. 2) in 31% and <1% yields, respectively. This necessitated the separation of the main product *O*-decyl-Ptr **1** to investigate it, including physicochemical and photochemical properties (14,15). In addition, to develop a new long alkane chain pterin that leaves the pterin core largely unperturbed, we synthesized and photochemically characterized decyl pterin-6-carboxyl ester (CapC **5**) (Fig. 2) that preserves the pterin amide group. CapC contains a decyl-chain at the carboxylic acid position and a condensed DMF molecule at the N^2 position (16). This compound is capable of the general triple action not only as a membrane intercalator, but also fluorophore and $^1O_2$ sensitizer, leading to a "self-monitoring" membrane fluorescent probe and a membrane photodamaging agent. Other interesting examples of alkylation of heterocyclic compounds can be found in the literature (17).

Thus, we hypothesized that Lum could provide for new lipophilic structures without DMF condensation for facile investigation of its physicochemical and photochemical properties. Indeed, the alkylated pterins showed not only big improvements in solubility in organic solvents, but also resided in rather than transported through membranes. The photophysics data were also encouraging, compared to native Ptr, decyl-pterins had efficient intersystem crossing to the triplet excited state and produced singlet molecular oxygen ($^1O_2$) with high quantum yields thereby reacting with PUFAs to form hydroperoxides. Indeed, we observed the photosensitized oxidation of phospholipids by *O*-decyl-Ptr. Here, vesicles of phosphatidylcholine rich in PUFAs were used (18). *O*-Decyl-Ptr was found to be much more efficient photosensitizer of lipids than Ptr, attributed to its affinity with the lipid membrane causing prompt lipid peroxidation. The results were in good agreement with other studies performed with photosensitizers able to bind lipid membranes (19,20).

<Figure 2>

Here, we present experimental and theoretical studies on decyl-chain conjugation to Lum to increase its solubility in organic solvents and to study their photophysical activity. Lipophilic enhancement of lumazines has not been studied previously, nor have lipophilic derivatives or regioselective alkylations been studied. We now report a study on new alkylated-lumazines, including (i) characterizations, (ii) molecular orbital (MO) and Mayr's nucleophilicity parameter *N* analyses to help rationalize the alkylation pattern of lumazines (*N*-decylation but not *O*-decylation), (iii) absorption and emission properties, and (iv) thermal and

photochemical stabilities. The behavior and properties of the new decyl chain-lumazine conjugates are compared to those of their precursor Lum and to decyl chain-pterin conjugates.

MATERIALS AND METHODS

Chemicals. Lumazine (Lum) was from Schircks Laboratories. 1-Iododecane was from Sigma. *N,N*-Dimethylformamide (DMF), dichloromethane (DCM), and chloroform-*d* were from Cicarelli, and potassium carbonate (K_2CO_3) was obtained from Biopack. Acetonitrile and methanol were from J. T. Baker, both of them were HPLC grade. Water was purified using a deionization system.

Absorption Measurements. Electronic absorption spectra were recorded on a Shimadzu UV-1800 spectrophotometer, using quartz cells of 0.4 or 1 cm optical path length.

Nuclear Magnetic Resonance spectroscopy. Spectra were recorded on a Bruker Avance Neo 500 (500 MHz for ^{1}H and 125.1 MHz for ^{13}C). Chemical shifts (δ) are given in ppm downfield from TMS as the internal standard. Coupling constant (*J*) values are in Hz.

Synthesis of alkyl lumazines. To a solution of lumazine (10 mg, 0.061 mmol) in DMF (14 mL), powder potassium carbonate (8.4 mg, 0.061 mmol) was added. The mixture was sonicated and sparged with nitrogen for 20 min and then, 1-iododecane (78.5 μL, 0.366 mmol) was added. The reaction mixture was placed into an oil bath and was stirred at 70ºC for 24 h. The solution was cooled at room temperature, and the solvent was evaporated to dryness under vacuum, providing a solid residue. This solid residue was treated with a saturated solution of NaCl (50mL) and then extracted with DCM (3 x 50 mL). The organic layers were combined, dried over Na_2SO_4, filtered, and evaporated to dryness. The solid obtained was purified by silica gel column chromatography (eluent: DCM 100% followed by DCM-MeOH mixtures). From the eluted fractions, the products 1-decyl-Lum **6a** and 1,3-*bis*-decyl-Lum **7a** were isolated and characterized by means of physical and spectroscopic methods.

1-Decyl-Lum (1-decylpteridine-2,4(1H,3H)-dione, 6a*).* White solid. Yield: 4.9 mg (26%), purity 97 %. R_f (methanol/DCM 5:95 v/v) 0.42. mp: 125 - 127 ºC. ^{1}H NMR (500 MHz, $CDCl_3$) δ 9.01 (s, 1H, NH), 8.66 (d, *J* = 2.2 Hz,1H), 8.59 (d, *J* = 2.2 Hz, 1H), 4.27 (t, *J* = 7.64 Hz, 2H), 1.71 (q, *J* = 7.7 Hz, 2H), 1.45 – 1.17 (m; 14H), 0.87 (t, *J* = 6.9 Hz, 3H). ^{13}C NMR (126 MHz, $CDCl_3$) δ 159.6, 149.5, 149.3, 147.9, 140.4, 128.7, 42.4, 32.0; 29.7, 29.6, 29.4, 29.4, 27.8, 26.9, 22.8, 14.3. LCMS (ESI) *m/z* calcd for $C_{16}H_{23}N_4O_2$ $[M^+H^+]$= 305.1978, found 305.1984. Molar absorption coefficient (ε) in MeOH at 331 nm is 5855 $M^{-1}cm^{-1}$.

1,3-Bis-decyl-Lum (1,3-didecylpteridine-2,4(1H,3H)-dione, 7a). White crystalline solid needle-shape. Yield: 14.5 mg (54%), purity 97 %. R_f (methanol/DCM 5:95 v/v) 0.90. mp: 54 – 53 ºC. ^{1}H NMR (500 MHz, $CDCl_3$) δ 8.62 (d, J = 2.3 Hz, 1H), 8.57 (d, J = 2.3 Hz, 1H), 4.30 (t, J = 7.65 Hz, 2H), 4.11 (t, J = 7.6 Hz, 2H), 1.74 – 1.66 (m, 4H), 1.42 – 1.21 (m; 28 H), 0.88 (t, J = 6.9 Hz, 3H), 0.87 (t, J = 6.4 Hz, 3H). ^{13}C NMR (126 MHz, $CDCl_3$) δ 159.9, 150.2, 148.2, 147.6, 140.3, 128.3, 42.9, 42.7, 32.0, 29.7, 29.5, 29.4, 27.9, 27.8, 27.1, 26.9, 22.8, 14.3. LCMS (ESI) *m/z* calcd for $C_{26}H_{44}N_4O_2$ $[M^+H^+]$= 445.3537, found 445.3549. Molar absorption coefficient (ε) in MeOH at 333 nm is 5942 $M^{-1}cm^{-1}$.

Computational methods. Calculations were performed with the Gaussian 16.C.01 program package (21) and visualized with Gaussview 5.0 (22). Optimizations were carried out with the B3LYP functional and the D95(d,p) basis set. An ultrafine grid was used and frequency calculations were performed to confirm that the optimized structures were local minima.

Chromatographic analysis. **High-performance liquid chromatography (HPLC).** A Prominence equipment from Shimadzu (solvent delivery module LC-20AT, on-line degasser DGU-20A5, communications bus module CBM-20, auto sampler SIL-20A HT, column oven CTO-10AS VP and photodiode array (PDA) detector SPD-M20A) was employed. The samples before and after irradiation were analyzed. A Synergi Polar-RP analytical column (ether-linked phenyl phase with polar endcapping, 150 x 4.6 mm, 4 μm, Phenomenex) was used for separation. 100 % MeOH was used as mobile phase with a flow of 0.3 mL min^{-1}.

Mass spectrometry analysis. The liquid chromatography equipment coupled to mass spectrometry (LCMS) system was equipped with an UPLC chromatograph (ACQUITY UPLC, Waters), and a UV/vis detector (Acquity TUV), coupled to a quadrupole time-of-flight mass spectrometer (Xevo G2-QTof-MS, Waters), equipped with an electrospray ionization source (ESI). UPLC analyses were performed using the Acquity UPLC BEH Phenyl column (1.7 μm, 2.1 x 50 mm, Waters) and gradient elution starting with 40% water and 60% of acetonitrile and finishing with 80% acetonitrile, at a flow rate of 0.2 mL min^{-1}. The mass spectrometer was operated in positive mode with a capillary voltage of 2.5 kV, the cone voltage of 30 V, the cone gas flow of 20 L h^{-1}, the source temperature set to 130 °C and the desolvation temperature set to 450 °C.

Fluorescence measurements. Steady-state fluorescence measurements were performed at room temperature using a single-photon-counting equipment FL3TCSPC-SP (Horiba Jobin Yvon), described elsewhere (23). To obtain the fluorescence spectra, the sample solution in a quartz cell was irradiated with a CW 450W Xenon source through an excitation monochromator and

the luminescence, after passing through an emission monochromator, was registered at 90º with respect to the incident beam using a room-temperature R928P detector. The fluorescence quantum yields (Φ_F) were determined from the corrected fluorescence spectra using Equation 1:

$$\Phi_F = \Phi_F^R I A^R n^{2R} / I^R A n^2 \quad (1)$$

where I is the integrated intensity, A is the absorbance at the excitation wavelength (λ_{exc}), n is the refraction index of each solvent and the superscript R refers to the reference fluorophore. In our experiments Lum in acidic aqueous solution (Φ_F= 0.08) (32) and *N*-decyl-Ptr in acetonitrile (Φ_F= 0.043) (14). were used as references. To avoid inner filter effects, the absorbance of the solutions, at the excitation wavelength, was kept below 0.10. Spectra were corrected for wavelength-dependent emission profiles with corrections factors supplied by the manufacturer and using the software FluorEssence™ version 3.9 (Horiba Jobin Yvon).

Steady-state irradiation. The continuous photolysis of compounds in air-equilibrated solutions was carried out irradiating in quartz cells (0.4 cm optical path length). One Rayonet RPR 3500 lamps (Southern N.E. Ultraviolet Co.) with emission centered at 350 nm [band width (fwhm) 20 nm] was employed as radiation source.

RESULTS AND DISCUSSION

Synthesis and Characterization of *Mono*- and *Bis*-Decylated Lumazines

Two new decyl-lumazines were synthesized by reacting Lum in a bimolecular nucleophilic substitution (S_N2) reaction. Under basic conditions with K_2CO_3, Lum reacted with 1-iododecane in DMF solvent under heating at 70 °C for 24 h (Scheme 1). As we will see, the structures of the products were 1-decyl-Lum **6a** and 1,3-*bis*-decyl-Lum **7a**, formed in 26% and 54% yields. The products were separated by column chromatography from the reaction mixture due to their distinct R_f values [0.42 for mono- *vs* 0.90 for dialkylated Lum, using as mobile phase dichloromethane (DCM): methanol (MeOH) 95:5]. The purity of the compounds was higher than 98% according to HPLC controls. As anticipated, the alkylated lumazines showed enhanced solubility in organic solvents in comparison with native Lum, as is the case for alkylated pterins compared to native Ptr (14,15).

<Scheme 1>

The structures of 1-decyl-Lum **6a** and 1,3-*bis*-decyl-Lum **7a** were deduced based on analytical and spectroscopic data below, as we will see. Liquid Chromatography-Mass Spectrometry (LCMS) provided high-resolution mass evidence for the monoalkylation of Lum (MS calcd. for $C_{16}H_{25}N_4O_2$ $[M^+H^+]$ = 305.1978, found 305.1984). LCMS also provided high-

resolution mass evidence for the dialkylation of Lum (MS calcd. for $C_{26}H_{44}N_4O_2$ [M^+H^+] = 445.3537, found 445.3549).

The elucidation of the chemical structures of the mono- and dialkylated lumazines came from 1D and 2D NMR. In particular, in the ^1H NMR spectrum ($CDCl_3$) of 1-decyl-Lum **6a** the methylene α protons of the decyl chain attached to the N^1 of the heterocycle are clearly found at 4.27 ppm, while the methylene β protons are observed at 1.71 ppm. Likewise, the methyl ω protons are found at 0.87 ppm, while the bulk methylene protons are observed as a wide peak in the range of 1.45 – 1.17 ppm. The NMR spectroscopic behavior observed for 1,3-*bis*-decyl-Lum **7a** clearly showed that two decyl chains are attached to the Lum moiety. In fact, two doubled-set of protons are observed, and for methylene α protons two distinct triplets are found at 4.30 and 4.11 ppm, respectively, and the same result was observed for the methyl ω protons which are located at 0.88 ppm and 0.87 ppm, respectively.

Conclusive evidence that the monoalkylated lumazine is 1-decyl-Lum **6a** and the dialkylated lumazine is 1,3-*bis*-decyl-Lum **7a** is based on 2D NMR, namely HSQC, HMBC and NOESY methodologies (see Supporting Information). Figure 3 shows the partial 2D NMR HMBC and NOESY spectra of 1-decyl-Lum **6a**. As can be seen in Fig. 3a, a nice correlation between C^{8a} (149.5 ppm) of the Lum moiety and proton α of the alkyl chain was observed indicating that the decyl chain is univocally attached at N^1 (see the inset of the chemical structure of 1-decyl-Lum **6a**). Moreover, correlation between the proton α and the carbonyl signal located at 149.3 ppm reinforces the elucidated structure. A NOESY experiment also showed a correlation between the amine proton (N^1-H) at 9.01 ppm with the β-proton of the decyl chain at 1.71 ppm (Fig. 3b).

<Figure 3>

From Fig. 4, the partial 2D NMR (HMBC) spectrum provides evidence for 1,3-*bis*-decyl-Lum **7a**, in which two distinct and clear correlations exist between proton and carbon signals. Indeed, the signal of the methylene proton α at 4.30 ppm of the decyl chain attached to the N^1 of the Lum moiety (orange arrow) correlates with both carbon atoms C^2 and C^{8a} of the heterocyclic nucleus at 150.2 ppm and 148.2 ppm, respectively. Likewise, the other decyl chain attached to the N^3 of the Lum moiety (blue arrows) shows that the methylene proton α at 4.11 ppm correlates with the carbon atoms of the carbonyl groups C^2 and C^1 at 150.2 ppm and 159.9 ppm. In this way, the structure of 1,3-*bis*-decyl-Lum was univocally elucidated.

<Figure 4>

It is noteworthy to mention here that no *O*-alkylation of Lum was observed in the reaction. This is an intriguing result in that Lum behaves differently from Ptr since *N*-alkylation

is favored on the former and *O*-alkylation is favored on the latter (14,15). The above experimental data show mono- and dialkylation in Lum trapping efficiency could not be fully explained by simple differences in mono-alkylation of pterin, and thus these differences might relate to aspects of the native structures. Thus, we turned to DFT calculations to study the properties of mono- and dialkylated lumazines (Fig. 5).

<Figure 5>

DFT Calculations

To help predict the alkylation pattern of Lum, we describe results with (1) molecular orbital (MO) theory, (2) Mayr's nucleophilicity parameter *N*, and (3) computed energetics.

B3LYP/D95(d,p) calculations for the highest occupied molecular orbital (HOMO) and lowest unoccupied molecular orbital (LUMO) calculations were carried out on the parent Lum, 1-decyl-Lum **6a**, 3-decyl-Lum **6b**, and 1,3-*bis*-decyl-Lum **7a** (Fig. 6). In contrast, Lum shows a node (*i.e.,* no electron density) at N^3, which implies little or no nucleophilicity for alkylation at this site. This MO analysis is consistent with the alkylation pattern that is observed experimentally. Furthermore, after alkylation occurs at N^1 of Lum to reach **6a**, a *p*-orbital then emerges on N^3, making it nucleophilic for alkylation at N^3 thereby reaching the dialkylated product **7a**.

These DFT results suggest that only the monoalkylated N^1 **6a** forms as an intermediate on the path to the dialkylated final product **7a**. The formation of monoalkylated N^3 **6b** is not feasible and does not serve as a primary product in the subsequent alkylation process to reach the dialkylated product **7a**. The HOMO on 1-decyl-Lum **6a** displays a contributing σ orbitals, as well as small but significant *p* orbital at the N^3 position, this predicts a route to di-alkylation. Similar to the HOMO of Lum, the HOMO of lumazine **6b** has a node at N^3. Let us comment further on the experimental percent yields of **6a** and **7a**, which is pertinent here. Lumazine (0.061 mmol) had reacted with a 6-fold excess of 1-iododecane (0.366 mmol) to form 26% yield of **6a**. Lumazine **7a** is formed in twice this yield, indicating there is good nucleophilicity at N^3 in **6a** as there is at N^1 in Lum.

<Figure 6>

B3LYP/D95(d,p) calculations were previously reported for the decylation of Ptr (15). We now employ B3LYP/D95(d,p) calculations to assess the energetics for the decylation of Lum. Our calculations focused on the gas-phase energetics. We find that the energetics of

decylated N^1 **6a** and N^3 **6b** are nearly the same (isoenergetic, Fig. 7). Lumazine **6a** with the N^1 substituted has a slightly higher energy than **6b** of 0.4 kcal/mol.

Gas-phase DFT calculations also predict the formation of N^1,N^3-dialkylated **7a**. Even though our experiments were carried out in DMF, which can stabilize polar species, the computed results show substantial differences that we do not attribute to solvent effects. Namely, other dialkylated combinations (N^1,O^2, N^1,O^4, O^2,O^4, N^3,O^2, and N^3,O^4) are less stable 15.6 to 32.1 kcal/mol (Fig. S16, Supporting Information).

Experimentally, nucleophilic substitution at N^1 is preferred over N^3 in Lum suggesting a process where **6a** is consumed rapidly in the formation of dialkylated product **7a**.

The alkylation reaction of Lum can be analyzed using Mayr's nucleophilicity parameter N (24). The nucleophilicity of sulfonamide anion (R─SO_2─NH^-), amide anion [R─C(=O)─NH^-], and imide anion [R─C(=O)─NH^-─C(=O)─R'] possess relatively small N parameters from $15<N<22$. These three anions are less reactive than structurally similar enolate anions of the same pK_{aH}, which may be attributed to the resonance stabilization of only one of the two lone pair electrons in the sulfonamide, amide, and imide anions. A key facet is that amide are n-nucleophiles while enolate anions are π-nucleophiles and hence they bear distinct reactivity toward electrophiles. Scheme 2 depicts two possible anionic lumazines under basic conditions, namely N^1-Lum anion and N^3-Lum anion. Using Mayr's nucleophilicity parameter N, (24) we can rationalize that the N^1-Lum anion will have an N of ~22, which is more nucleophilic compared to the N^3-Lum anion with an N of ~17, predicting the formation of 1-decyl-Lum **6a** over 3-decyl-Lum **6b**.

Scheme 2 shows two different paths to reach 1,3-*bis*-decyl-Lum **7a**, the sequence path (i) and (ii) and the sequence path (iii) and (iv). Starting from Lum N^1-anion which is the best nucleophile based on Mayr's parameter N of ~22, for the S_N2 reaction between N^1-anion and decyl iodide occurs efficiently and fast (path (i)) providing 1-decyl-Lum **6a** that accumulates in the reaction mixture. Because the reaction is held under basic conditions, **6a** N^3-anion, which is a poorer nucleophile with an N of ~17 and thus will react slowly with another equivalent of decyl iodide to provide 1,3-*bis*-decyl-Lum **7a** according to path (ii). These sequences explain why **6a** is detected in the reaction mixture together with **7a**. On the other hand, the sequences paths (iii) and (iv) show an alternative route to **7a**. Here, Lum N^3-anion reacts slowly with decyl iodide to reach **6b** (path (iii)) that in turn reacts rapidly with another equivalent of decyl iodide (path (iv)) to provide **7a**. Thus, it can be readily rationalized that **6b** does not build up during the alkylation reaction because as soon as it forms, it is rapidly consumed to give **7a**. Therefore, we can conclude that the theoretical calculations in term of molecular orbital (MO) theory

(HOMO – LUMO analysis), and analysis in terms of Mayr's nucleophilicity parameter *N* lead to a similar conclusion in the accumulation of **6a** and rapid consumption of **6b**, which can explain clearly the experimental results obtained during the alkylation reaction of Lum under basic conditions.

Let us now discuss the competition between *N*-alkylation and *O*-alkylation of Lum. An analogy is with amide and imide anions as ambident nucleophiles, where attack at oxygen is also conceivable. Indeed, alkylation reaction of amides under neutral conditions often lead to both *O*- and *N*-alkylation products, however, amide anions typically react with electrophiles for *N*-alkylation products (25,26,27). In addition, *O*-alkylation reaction of amide anions has been observed when silver salts were employed as additives and rationalization of this behavior was attributed to the silver ion enhancement of the electrophile center favoring the attack of the more electronegative oxygen atom (28,29,30). Figure 7 shows that **6a** with the N^1 substituted has a slightly higher energy of 0.4 kcal/mol than **6b** with the N^3 substituted. But in contrast to alkylation at either nitrogen N^1 or N^3, which are thermodynamic products, lumazines **6c** and **6d** with substitution at O^2 and O^4, respectively, are computed to be substantially higher in energy (23.5 and 15.3 kcal/mol) than **6b**. Natural population analysis (NPA) calculations also show that Lum increases in negative charge density on O^2 and O^4 as the anion, but lumazines **6c** and **6d** are not observed experimentally, presumably due to these high kinetic energies. Therefore, we rationalize thermodynamics as governing the regioselectivity of Lum via *N*-alkylation as favored over the *O*-alkylation.

<Figure 7>

< Scheme 2>

Spectroscopic properties of Lum, 6a and 7a

Lum in aqueous solutions presents several acid-base equilibria, the equilibrium between the neutral and the mono-anionic form (Lum and Lum(-H)$^-$, respectively; Scheme 3) being the most relevant one at physiological pH, with a pK_a of 7.95 (31). The singlet excited state of the neutral form ^{1}Lum* is much more acidic than the ground state and in neutral or slightly acidic solutions undergoes fast deprotonation at N^3 (32). Therefore, when the neutral form of Lum is excited, the emission of the anionic form of the excited state (^{1}Lum(-H)$^{-*}$) is observed (Scheme 3). Consequently, changes in the pH of an aqueous solution of Lum do not lead to a modification of the emission spectra. For example, the normalized emission spectrum of an aqueous solution at pH 7, where the neutral form predominates, is equal to the normalized emission spectra of a solution at pH 9, where the anionic form predominates. In both cases,

$^1Lum(-H)^{-*}$ is the species responsible for the emission and a fluorescence band centered at *ca* 460 nm is registered (Fig. 8a).

< Scheme 3>

As expected, the absorption spectrum of Lum in MeOH (Fig. 8b) was very similar to the spectrum of the neutral form in H_2O (Fig. 8a). It is worth mentioning that the absorption band of lower energy of the spectrum of the anionic form is red shifted respect to the corresponding band of the neutral form (33). On the other hand, the corresponding emission spectrum of Lum in MeOH (Fig. 8b) showed a main band centered at *ca* 380 nm and blue-shifted respect to the emission spectrum in H_2O (Fig. 8a), and other less intense emission band matching the spectrum in H_2O. This emission behavior can be explained considering that, as expected, $^1Lum^*$ does not undergo complete deprotonation in MeOH and, consequently, the emission of both acid-base forms ($^1Lum^*$ and $^1Lum(-H)^{-*}$, Scheme 3) are observed, that of $^1Lum^*$ being the most intense. To test this hypothesis, K_2CO_3 was added to the solution and indeed led to the deprotonation depicted in Scheme 3. Under these basic conditions only the emission of $^1Lum(-H)^{-*}$ was observed (Fig. 8b).

<Figure 8>

The absorption spectra of 1-decyl-Lum **6a** and 1,3-*bis*-decyl-Lum **7a** were recorded in MeOH (Fig. 8c and 8d, respectively) and resulted similar to the corresponding spectrum of Lum in the same solvent. These results indicate that the alkylation of the Lum moiety does not significantly affect the electronic distribution of the neutral form, which is reasonable considering the structure proposed for the substituted derivatives (Scheme 1). As expected, the emission spectra of 1-decyl-Lum **6a** and 1,3-*bis*-decyl-Lum **7a** in MeOH (Fig. 8c and 8d, respectively), are also similar to the emission spectrum of Lum in MeOH, which we interpret as emission from the neutral form of the singlet excited state (equivalent to $^1Lum^*$ in Scheme 3). Moreover, fluorescence quantum yields (Φ_F) of compounds Lum, 1-decyl-Lum **6a** and 1,3-*bis*-decyl-Lum **7a** in MeOH were obtained and are shown in Table 1. It is worth mentioning that the Φ_F values of alkylated compounds and Lum in MeOH are much lower than that corresponding to the parent Lum in H_2O (32). In organic solvents, the lack of a deprotonation pathway means there is no strong emission from the excited anionic form ($^1Lum(-H)^{-*}$ for Lum, Scheme 3), which limits the emission to the weak fluorescence of the excited state of the neutral form ($^1Lum^*$ for Lum, Scheme 3). On the other hand, the Φ_F values of 1-decyl-Lum **6a** and 1,3-*bis*-decyl-Lum **7a** are also significantly higher than that of Lum in MeOH, but this difference cannot be easily explained in terms of chemical structure.

<Table 1>

Photochemical stability

The photochemical stability of 1-decyl-Lum **6a** and 1,3-*bis*-decyl-Lum **7a** was evaluated in air-equilibrated MeOH solutions. The samples were exposed to UV-A irradiation for different periods of time and subsequently injected in the HPLC equipment to determine the concentration of the alkyl-lumazines. As shown in Fig. 9, the concentration of both compounds rapidly decreased upon irradiation, with a similar rate of photodegradation. Since Lum is a photostable compound, as reported previously (33), it can be concluded that alkylation of Lum moiety enhanced the photochemical reactivity, meaning alkylation leads to a higher susceptibility to photodegradation. Also, a similar behavior was observed for alkyl-pterin derivatives (14).

The behavior of alkyl-lumazines was compared to that of *O*-decyl-Ptr. Since the absorption spectrum of this compound is different to those of 1-decyl-Lum **6a** and 1,3-*bis*-decyl-Lum **7a**, the three initial solutions were adjusted at the same absorbance (0.23) at 350 nm (maximum of the lamp spectrum). In this way the rate of photons absorbed for all compounds was quiet similar in our experiments. Under these experimental conditions, the rate of photodegradation of both alkyl-lumazines was significantly higher than that of *O*-decyl-Ptr (Fig. 9).

<Figure 9>

CONCLUSIONS

To build on top of our prior alkylation work with pterins (14,15), we have now acquired new insight into the alkylation of lumazines. We have synthesized and photochemically characterized two decyl chain lumazine conjugates, 1-decylpteridine-2,4(1,3*H*)-dione **6a** and 1,3-didecylpteridine-2,4(1,3*H*)-dione **7a**, which form from lumazine through nucleophilic substitution (S_N2) reactions. *N*-Alkylation of lumazine is observed (thermodynamic control), which differs from pterins, where *O*-alkylation is preferred (kinetic control) (14,15). Compared to Lum, lumazines **6a** and **7a** have similar absorption spectra, possess slightly higher fluorescence quantum yields, and substantially higher organic solvent solubilities, but compared to *O*-decyl-Ptr, lumazines **6a** and **7a** have lower photostability under UVA irradiation.

The results with pterins and now with lumazines serve as a reference point for how alkylation patters at *O*- vs *N*- in the former and di- vs mono- in the latter can further advance the lipophilic character of sensitizers. Our work provides a platform on which further research can be built to expand the use of pteridines in membrane-bound photosensitization reactions.

ACKNOWLEDGEMENTS. The present work was partially supported by Consejo Nacional de Investigaciones Científicas y Técnicas (CONICET-Grant P-UE 2017 22920170100100CO), Agencia Nacional de Promoción Científica y Tecnológica (ANPCyT-Grants PICT 2015-1988, PICT 2016-1189 and PICT 2017-0925), Universidad Nacional de La Plata (UNLP-Grant 11/X840 and 11/X858). Authors thank CONICET and National Science Foundation (NSF) for supporting their collaboration through a Bilateral Cooperation Programme Level I. MJS and MIQ thank CONICET for doctoral research fellowships, MNU thanks CONICET for a postdoctoral fellowship. PLS, SB, MV and AHT are research members of CONICET. This work used Comet, the Extreme Science and Engineering Discovery Environment (XSEDE) cluster at the San Diego Supercomputer Center, which is supported by NSF grant number ACI-1548562 through allocation CHE180060. AG acknowledges support from the NSF (CHE-1856765), and DD and EMG also acknowledge support from the NSF (CHE-1956098).

SUPPORTING INFORMATION

Additional supporting information may be found online in the Supporting Information section at the end of the article:

Figure S1. 500 MHz ^{1}H-NMR spectrum of N^{1}-decyl-Lum in $CDCl_3$.

Figure S2. 127.5 MHz ^{13}C-NMR spectrum of N^{1}-decyl-Lum in $CDCl_3$.

Figure S3. 500 MHz HSQC-DEPT spectrum of N^{1}-decyl-Lum in $CDCl_3$.

Figure S4. 500 MHz HMBC spectrum of N^{1}-decyl-Lum in $CDCl_3$.

Figure S5. 500 MHz NOESY spectrum of N1-decyl-Lum in CDCl3.

Figure S6. LCMS spectrum of N1-decyl-Lum.

Figure S7. LCMS-MS spectrum of N1-decyl-Lum.

Figure S8. 500 MHz 1H-NMR spectrum of N1,N3-bis-decyl-Lum in CDCl3.

Figure S9. 127.5 MHz 13C-NMR spectrum of N1,N3-bis-decyl-Lum in CDCl3.

Figure S10. 500 MHz HSQC-DEPT spectrum of N1,N3-bis-decyl-Lum in CDCl3.

Figure S11. 500 MHz HMBC spectrum of N1,N3-bis-decyl-Lum in CDCl3.

Figure S12. 500 MHz NOESY spectrum of N1,N3-bis-decyl-Lum in CDCl3.

Figure S13. LCMS spectrum of N1,N3-bis-decyl-Lum.

Figure S14. LCMS-MS spectrum of N1,N3-bis-decyl-Lum. B3LYP/D95(d,p) Computed Data and Coordinates.

Figure S15. B3LYP/D95(d,p) Computed Energies of Di-substituted Lumazines.

Figure S16. B3LYP/D95(d,p) Computed Energies of Tautomeric Compounds.

REFERENCES

1. Kappock, T. J. and J. P. Caradonna (1996) Pterin-dependent amino acid hydroxylases. *Chem. Rev.* **96**, 2659-2756.

2. Rembold, H. and W. L. Gyure (1972) Biochemistry of the Pteridines. *Angew. Chem., Int. Ed. Engl.* **11**, 1061–1072.

3. Rembold, H., V. Chandrashekar and P. Sudershan (1971) Catabolism of pteridine cofactors: IV. *In vivo* catabolism of reduced pterins in rats, *Biochim. Biophys. Acta* **237**, 365-368.

4. Kis K., K. Kugelbrey and A. Bacher (2001) Biosynthesis of Riboflavin. The reaction catalyzed by 6,7-dimethyl-8-ribityllumazine synthase can proceed without enzymatic catalysis under physiological conditions. *J. Org. Chem.* **66**, 2555–2559.

5. D. J. Brown, Introduction to the Pteridines, in *The Chemistry of Heterocyclic Compounds, Part 3, Volume 24, Fused Pyrimidines: Pteridines*, ed. D. J. Brown, John Wiley and Sons, New York, 1988, ch. 6, pp. 1-42.

6. Serrano, M. P., M. Vignoni, M. L. Dántola, E. Oliveros, C. Lorente and A. H. Thomas (2011) Emission properties of dihydropterins in aqueous solutions. *Phys. Chem. Chem. Phys.* **13**, 7419–7425.

7. Lorente, C. and A. H. Thomas (2006) Photophysics and photochemistry of pterins in aqueous solution. *Acc. Chem. Res.* **39**, 395-402.

8. Dántola, M. L., L. O. Reid, C. Castaño, C. Lorente, E. Oliveros and A. H. Thomas (2017) Photosensitization of peptides and proteins by pterin derivatives. *Pteridines* **28**, 105–114.

9. Denofrio, M. P., A. H. Thomas and C. Lorente (2010) Oxidation of 2'-deoxyadenosine 5'-monophosphate photoinduced by Lumazine. *J. Phys. Chem. A* **114**, 10944–10950.

10. Denofrio, M. P., S. Hatz, C. Lorente, F. M. Cabrerizo, P. R. Ogilby and A. H. Thomas (2009) The photosensitizing activity of lumazine using 2'-deoxyguanosine 5'-monophosphate and HeLa cells as targets. *Photochem. Photobiol. Sci.* **8**, 1539-1549.

11. Denofrio, M. P., C. Lorente, T. Breitenbach, S. Hatz, F. M. Cabrerizo, A. H. Thomas and P.

R. Ogilby (2011) Photodynamic effects of pterin on HeLa Cells. *Photochem. Photobiol.* **87**, 862–866.

12. Miñán, A., C. Lorente, A. Ipiña, A. H. Thomas, M. Fernández Lorenzo de Mele and P. L. Schilardi (2015) Photodynamic inactivation induced by carboxypterin: a novel non-toxic bactericidal strategy against planktonic cells and biofilms of Staphylococcus aureus, *Biofouling* **31**, 459–468.

13. Thomas, A. H., Á. Catalá and M. Vignoni (2016) Soybean phosphatidylcholine liposomes as model membranes to study lipid peroxidation photoinduced by pterin. *Biochim. Biophys. Acta, Biomembr.* **1858**, 139-145.

14. Vignoni, M., N. Walalawela, S. M. Bonesi, A. Greer and A. H. Thomas (2018) Lipophilic decyl chain−pterin conjugates with sensitizer properties. *Mol. Pharm.* **15**, 798−807.

15. Walalawela, N., M. Vignoni, M. N. Urrutia, S. J. Belh, E. M. Greer, A. H. Thomas and A. Greer (2018) Kinetic control in the regioselective alkylation of pterin sensitizers: A synthetic, photochemical, and theoretical study. *Photochem. Photobiol.* **94**, 834−844.

16. Walalawela, N., M. N. Urrutia, A. H. Thomas, A. Greer and M. Vignoni (2019) Alkane chain-extended pterin through a pendent carboxylic acid acts as triple functioning fluorophore, $^1O_2$ sensitizer and membrane binder. *Photochem. Photobiol.* **95**, 1160–1168.

17. Abdulwahaab, B. H., B. P. Burke, J. Domarkas, J. D. Silversides, T. J. Prior and S. J. Archibald (2016) Mono- and bis-alkylation of glyoxal-bridged tetraazamacrocycles using mechanochemistry. *J. Org. Chem.* **81**, 890-898.

18. Vignoni, M., M. N. Urrutia, H. C. Junqueira, A. Greer, A. Reis, M. S. Baptista, R. Itri and A. H. Thomas (2018) Photooxidation of unilamellar vesicles by a lipophilic pterin: Deciphering biomembrane photodamage. *Langmuir* **34**, 15578−15586.

19. Bacellar, I. O. L., M. C. Oliveira, L. S. Dantas, E. B. Costa, H. C. Junqueira, W. K. Martins, A. M. Durantini, G. Cosa, P. Di Mascio, M. Wainwright, R. Miotto, R. M. Cordeiro, S.

Miyamoto and M. S. Baptista (2018) Photosensitized membrane permeabilization requires contact-dependent reactions between photosensitizer and lipids. *J. Am. Chem. Soc.* **140**, 9606-9615.

20. Tasso, T. T., J. C. Schlothauer, H. C. Junqueira, T. A. Matias, K. Araki, É. Liandra-Salvador, F. C. T. Antonio, P. Homem-de-Mello and M. S. Baptista (2019) Photobleaching efficiency parallels the enhancement of membrane damage for porphyrazine photosensitizers. *J. Am. Chem. Soc.* **141**, 15547-15556.

21. Gaussian 16, Revision C.01, Frisch, M. J.; Trucks, G. W.; Schlegel, H. B.; Scuseria, G. E.; Robb, M. A.; Cheeseman, J. R.; Scalmani, G.; Barone, V.; Petersson, G. A.; Nakatsuji, H.; Li, X.; Caricato, M.; Marenich, A. V.; Bloino, J.; Janesko, B. G.; Gomperts, R.; Mennucci, B.; Hratchian, H. P.; Ortiz, J. V.; Izmaylov, A. F.; Sonnenberg, J. L.; Williams-Young, D.; Ding, F.; Lipparini, F.; Egidi, F.; Goings, J.; Peng, B.; Petrone, A.; Henderson, T.; Ranasinghe, D.; Zakrzewski, V. G.; Gao, J.; Rega, N.; Zheng, G.; Liang, W.; Hada, M.; Ehara, M.; Toyota, K.; Fukuda, R.; Hasegawa, J.; Ishida, M.; Nakajima, T.; Honda, Y.; Kitao, O.; Nakai, H.; Vreven, T.; Throssell, K.; Montgomery, J. A., Jr.; Peralta, J. E.; Ogliaro, F.; Bearpark, M. J.; Heyd, J. J.; Brothers, E. N.; Kudin, K. N.; Staroverov, V. N.; Keith, T. A.; Kobayashi, R.; Normand, J.; Raghavachari, K.; Rendell, A. P.; Burant, J. C.; Iyengar, S. S.; Tomasi, J.; Cossi, M.; Millam, J. M.; Klene, M.; Adamo, C.; Cammi, R.; Ochterski, J. W.; Martin, R. L.; Morokuma, K.; Farkas, O.; Foresman, J. B.; Fox, D. J. Gaussian, Inc., Wallingford CT, 2016.

22. Dennington, R.; Keith, T.; Millam J. (2009) GaussView 5. Semichem Inc, Shawnee Mission KS.

23. Serrano, M. P., M. Vignoni, M. L. Dántola, E. Oliveros, C. Lorente and A. H. Thomas (2011) Emission properties of dihydropterins in aqueous solutions. *Phys. Chem. Chem. Phys.* **13**, 7419–7425.

24. Breugst, M., T. Tokuyasu and H. Mayr (2010) Nucleophilic reactivities of imide and amide

anions. *J. Org. Chem.* **75**, 5250-5258.

25. Challis, B. C.; Challis, J. in The Chemistry of Amides; Zabicky, J., Ed.; Interscience Publisher: London, UK, 1970; pp 731-858.

26. Stirling, C. J. M. (1960) 49. Intramolecular reactions of amides. Part II. Cyclisation of amides of ω-bromo-carboxylic, acids. *J. Chem. Soc.*, 255–262.

27. Dopp, D.; Dopp, H. Houben-Weyl Methods of Organic Chemistry, 1952-, 4th ed.; Thieme: Stuttgart, Germany, 1985; Vol. E5, pp 934-1135.

28. Koch, T. H., R. J. Sluski and R. H. Moseley (1973) Photochemical reactivity of keto imino ethers. IV. Type I and type II reactions. *J. Am. Chem. Soc.* **95**, 3957–3963.

29. Anderson, D. R., J. S. Keute, T. H. Koch and R. H. Moseley (1977) Di-tert-butyl nitroxide quenching of the photoaddition of olefins to the carbon-nitrogen double bond of 3-ethoxyisoindolenone. *J. Am. Chem. Soc.* **99**, 6332–6340.

30. Kornblum, N., R. A. Smiley, R. K. Blackwood and D. C. Iffland (1955) The mechanism of the reaction of silver nitrite with alkyl halides. The contrasting reactions of silver and alkali metal salts with alkyl halides. The alkylation of ambident anions. *J. Am. Chem. Soc.* **77**, 6269–6280.

31. Pfleiderer, W. (1957) I. Pteridine, über 2,4-dioxotetrahydropteridine. *Chem. Ber.* **90**, 2582–2587.

32. Klein, R. and I. Tatischeff (1987) Tautomerims and fluorescence of lumazine. *Potochem. Photobiol.* **45**, 55-65.

33. Denofrio, M. P., A. H. Thomas, A. M. Braun, E. Oliveros and C. Lorente (2008) Photochemical and photophysical properties of lumazine in aqueous solutions. *J. Photochem. Photobiol. A: Chem.* **200**, 282-286.

FIGURE CAPTIONS

Figure 1. Chemical structures of pteridine-2,4(1,3*H*)-dione or lumazine (Lum) and 2-aminopteridine-4(3*H*)-one or pterin (Ptr).

Figure 2. Chemical structures of previously reported mono-alkylated pterins: (1) 4-(decyloxy)pteridin-2-amine (*O*-decyl-Ptr), (2) *N'*-(4-(decyloxy)pteridin-2-yl)-*N,N*-dimethylformimidamide, (3) 2-amino-3-decylpteridin-4(3H)-one, (4) *N'*-(3-decyl-4-oxo-3,4-dihydropteridin-2-yl)-*N,N*-dimethylformimidamide, and (5) decyl(*E*)-2-(((dimethylamino) methylene)amino)-4-oxo-3,4- dihydropteridine-6-carboxylate (CapC).

Figure 3. Partial 2D NMR spectra of 1-decyl-Lum recorded **6a** in $CDCl_3$: (a) HMBC method and (b) NOESY method.

Figure 4. Partial 2D NMR spectra of 1,3-*bis*-decyl-Lum **7a** recorded in $CDCl_3$ using the HMBC method.

Figure 5. Structures of mono-alkylated lumazines (6a-d) and bis-alkylated lumazines (7a-f). The actual alkylated compounds are **6a** (1-decyl-Lum) and **7a** (1,3-*bis*-decyl-Lum).

Figure 6. B3LYP/D95(d,p) computed highest occupied molecular orbitals (HOMO) and lowest unoccupied molecular orbitals (LUMO) of Lum, **6a**, **6b**, and **7a**.

Figure 7. B3LYP/D95(d,p) computed free energies (ΔG) of mono-substituted lumazines at N^1, N^3, O^2 and O^4 sites in kcal/mol.

Figure 8. Absorption (green line) and normalized emission (brown line) spectra of a) Lum in H_2O (pH= 5.5, 46 µM, λ_{exc}= 325 nm), b) Lum in MeOH (49 µM, λ_{exc}= 325 nm), c) 1-decyl-Lum in MeOH (41 µM, λ_{exc}= 330 nm), d) 1,3-*bis*-decyl-Lum in MeOH (45 µM, λ_{exc}= 330 nm). The orange line in (b) corresponds to the normalized emission spectrum of Lum in MeOH after de addition of K_2CO_3 (3.6 mM).

Figure 9. Time evolution of concentrations of *O*-decyl-Ptr, 1-decyl-Lum **6a** and 1,3-*bis*-decyl-Lum **7a** in air-equilibrated MeOH solutions under UV-A irradiation. The three initial solutions were adjusted at the same absorbance (0.23) at 350 nm (maximum of the lamp spectrum), which corresponds to the following initial concentrations (C_0): [*O*-decyl-Ptr]$_0$= 43 µM, [1-decyl-Lum **6a**]$_0$= 33 µM and [1,3-*bis*-decyl-Lum **7a**]$_0$= 43 µM.

SCHEME CAPTIONS

Scheme 1. Synthesis of alkyllumazines: 1-decylpteridine-2,4(1,3*H*)-dione (1-decyl-Lum) **6a** and 1,3-didecylpteridine-2,4(1,3*H*)-dione (1,3-*bis*-decyl-Lum) **7a**. "Bulk" refers to the methylene groups within the alkyl chain that appear in a clustered region in the NMR spectrum.

Scheme 2. Proposed stepwise mechanism in the preparation of 1,3-*bis*-decyl-Lum **7a**.

Scheme 3. Acid-base equilibrium of Lum in aqueous solution and processes that take place when the neutral form is excited. Lum: neutral form, $Lum(-H)^-$: anionic form, hν: radiation absorbed, hν′: radiation emitted.

Table 1. Spectroscopic properties of Lum, 1-decyl-Lum 6a and 1,3-bis-decyl-Lum 7a in MeOH.

Compound	λ_{max}/ nm absorption	λ_{max}/ nm emission	Fluorescence quantum yield (Φ±SD)
Lum	231/324	379	0.004±0.002
1-decyl-Lum 6a	233/331	384	0.015±0.003
1,3-bis-decyl-Lum 7a	239/333	386	0.018±0.004

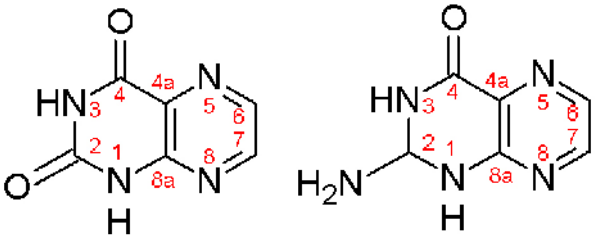

php_13310_f1.jpg

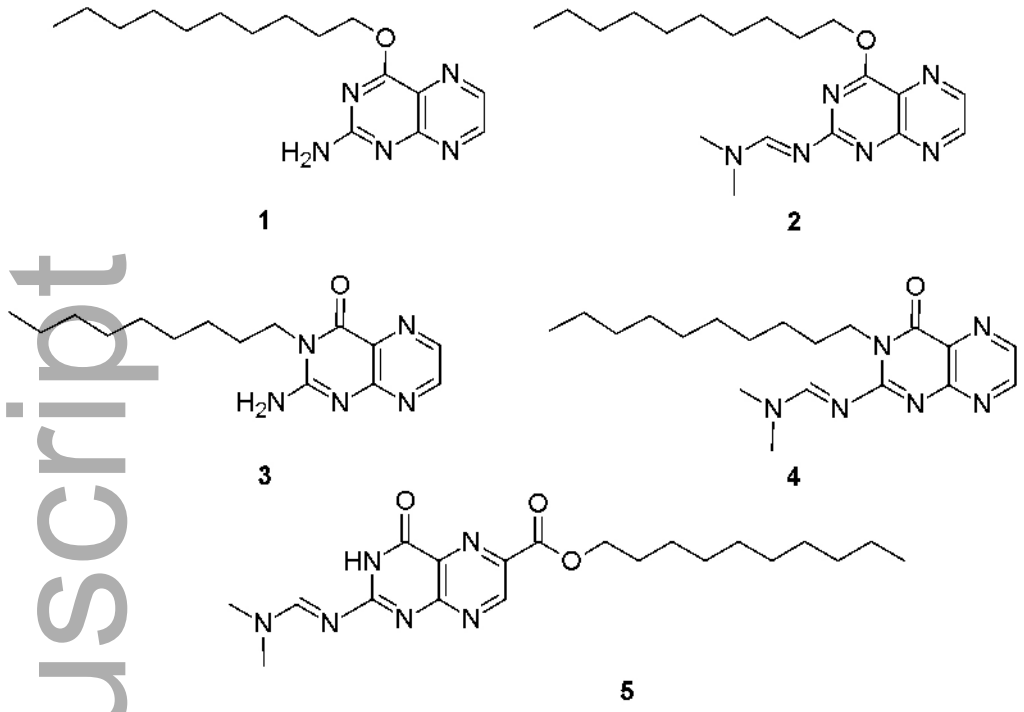

php_13310_f2.jpg

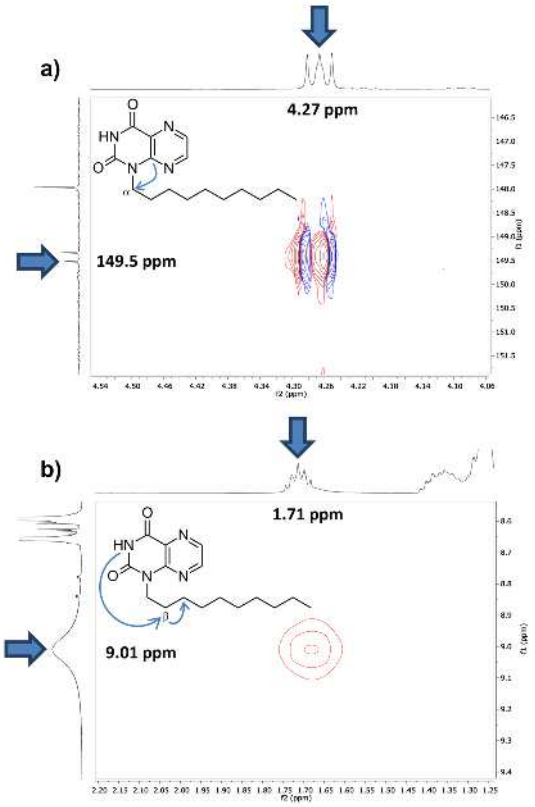

php_13310_f3.jpg

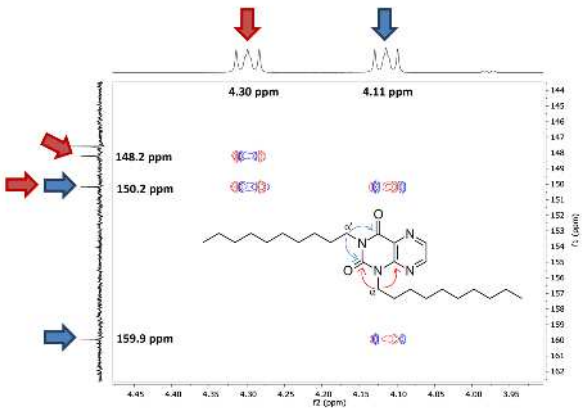

php_13310_f4.jpg

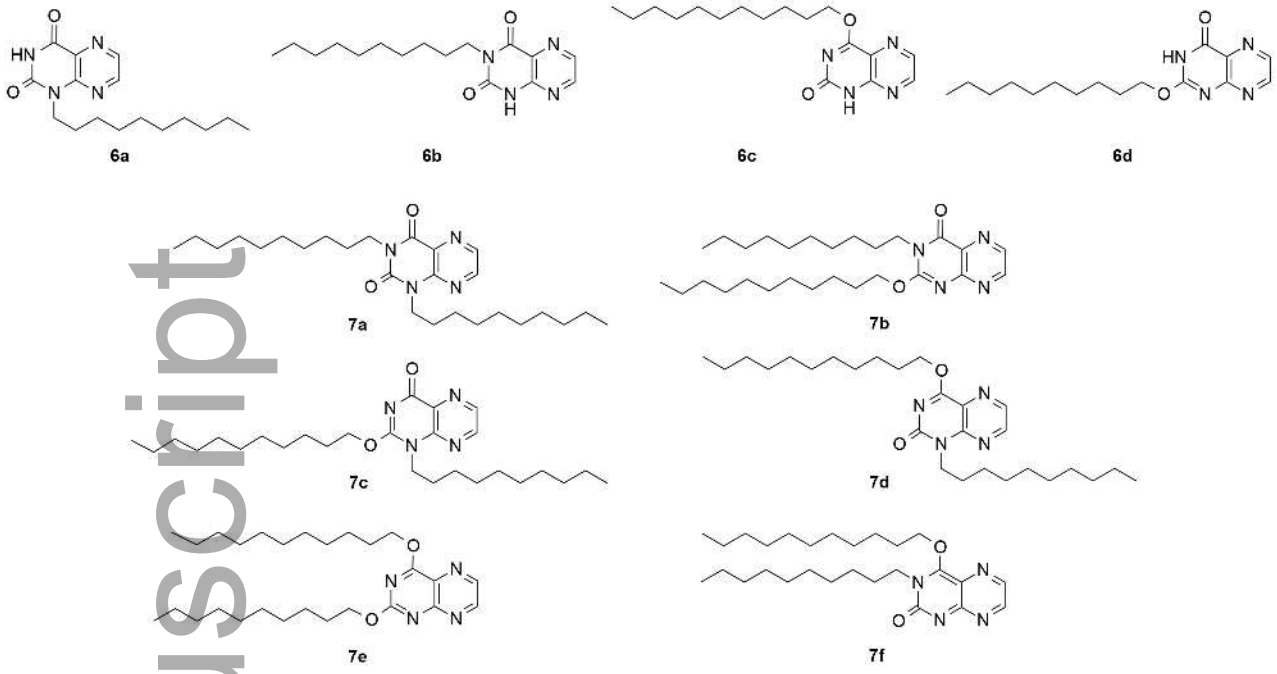

php_13310_f5.jpg

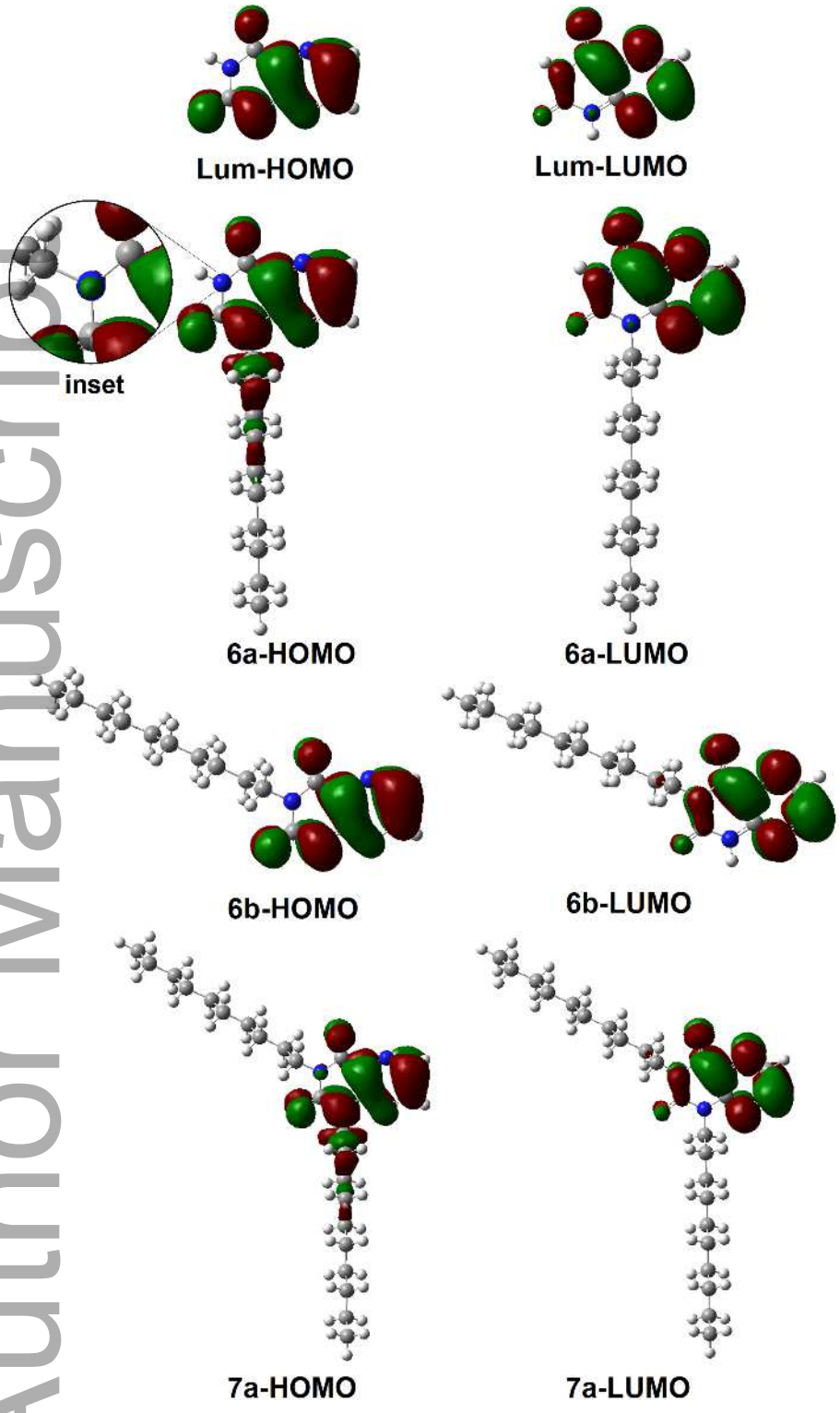

php_13310_f6.jpg

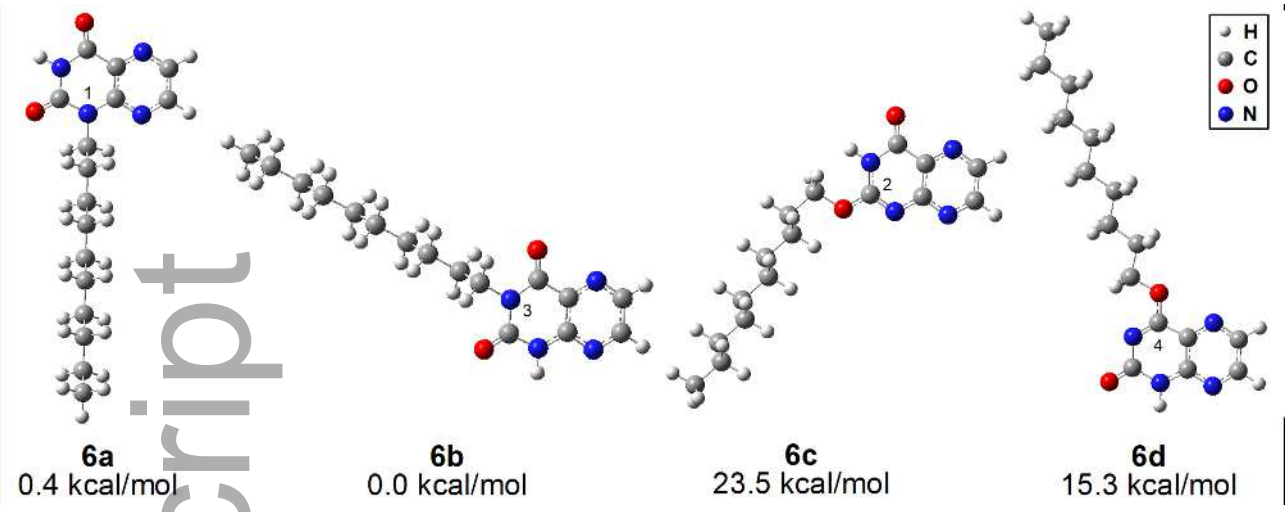

php_13310_f7.jpg

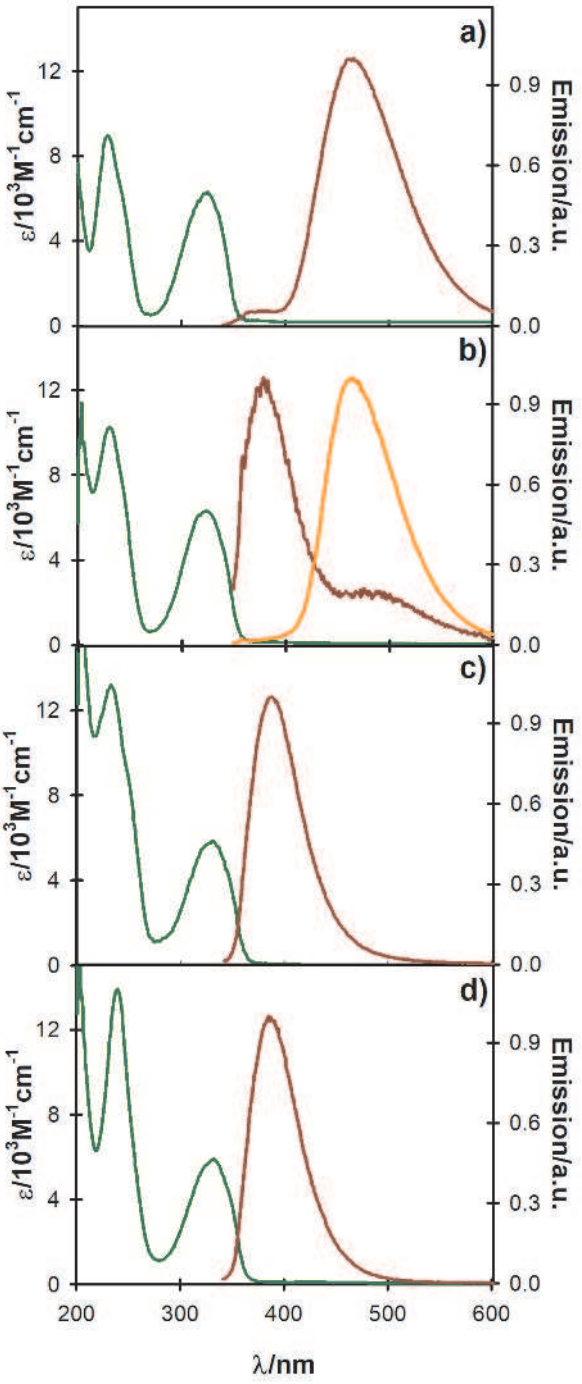

php_13310_f8.jpg

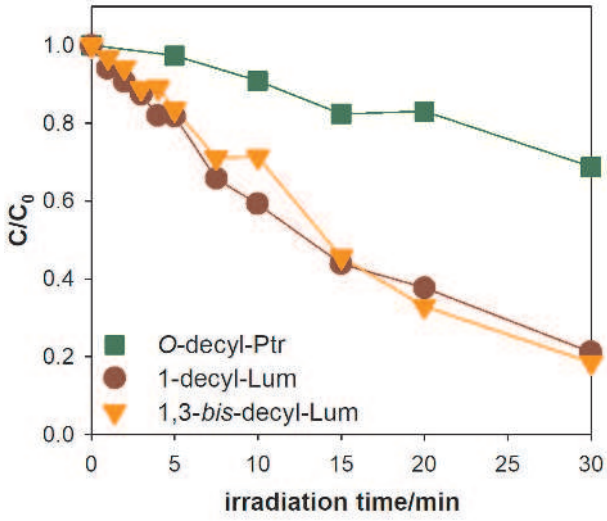

php_13310_f9.jpg